

Wigner solid pinning modes tuned by fractional quantum Hall states of a nearby layer

A. T. Hatke¹, H. Deng², Yang Liu², L. W. Engel^{1*},
L. N. Pfeiffer², K. W. West², K. W. Baldwin², M. Shayegan²

¹National High Magnetic Field Laboratory, Tallahassee, FL 32310, USA

²Dept. of Electrical Engineering, Princeton University, Princeton, NJ 08544, USA

* to whom correspondence should be addressed, email: engel@magnet.fsu.edu

We study a bilayer system hosting exotic many-body states of two-dimensional electron systems (2DESs) in close proximity but isolated from one another by a thin barrier. One 2DES has low electron density and forms a Wigner solid (WS) at high magnetic fields. The other has much higher density and, in the same field exhibits fractional quantum Hall states (FQHSs). The WS manifests microwave resonances which are understood as pinning modes, collective oscillations of the WS within the small but finite ubiquitous disorder. Our measurements reveal a striking evolution of the pinning mode frequencies of the WS layer with the formation of the FQHSs in the nearby layer, evincing a strong coupling between the WS pinning modes and the state of the 2DES in the adjacent layer, mediated by screening.

Introduction

Wigner solids occur when electron-electron interaction dominates the zero-point or thermal motion of the carriers. They can be accessed in extremely dilute systems in the absence of magnetic field or in high magnetic field (B) at sufficiently low Landau level filling, ν , at the termination of the FQHS series, where Wigner solids have long been expected (1–3). The magnetic-field-induced WS in a 2DES is of great interest and has been studied experimentally by a variety of different techniques including pinning mode spectroscopy (4–10), photoluminescence (11), transport (12–15), NMR (16) and time-dependent tunneling (17). As a state stabilized by electron-electron interaction, it can be expected that a WS is strongly affected by nearby screening layers or its dielectric environment. There are theoretical works (18, 19), concerning the phase diagram of a 2DES in the presence of a nearby metal gate, for which the gate carries image charge that renders electron-electron interaction dipolar at distances exceeding the gate separation. For a WS near a higher-dielectric-constant substrate, the screening is less strong, and image charge magnitude is less than $|e|$, as was studied (18, 20) for electrons separated from such substrates by thin He films.

Through pinning mode measurements (4–10), we study here a 2D WS screened by a much larger density 2DES in a neighboring quantum well (QW). Previous dc-transport studies (15) of such density-asymmetric double wells have demonstrated the existence of a triangular-lattice WS in close proximity to a majority layer with a composite fermion (CF) (21) metal near $\nu \sim 1/2$, by means of geometric resonance oscillations of the CFs acted on by the WS. Our work considers the reverse, and examines the effect of the CF metal and nearby majority-layer FQHSs on the statics and pinning-mode dynamics of the WS. In agreement with Ref. (15) we find strong pinning modes signifying the presence of a WS. The frequencies of these modes exhibit a remarkable dependence on the FQHSs formed in the nearby majority layer, allowing us to extract unique and unexpected information regarding the screening of the WS by this layer. The

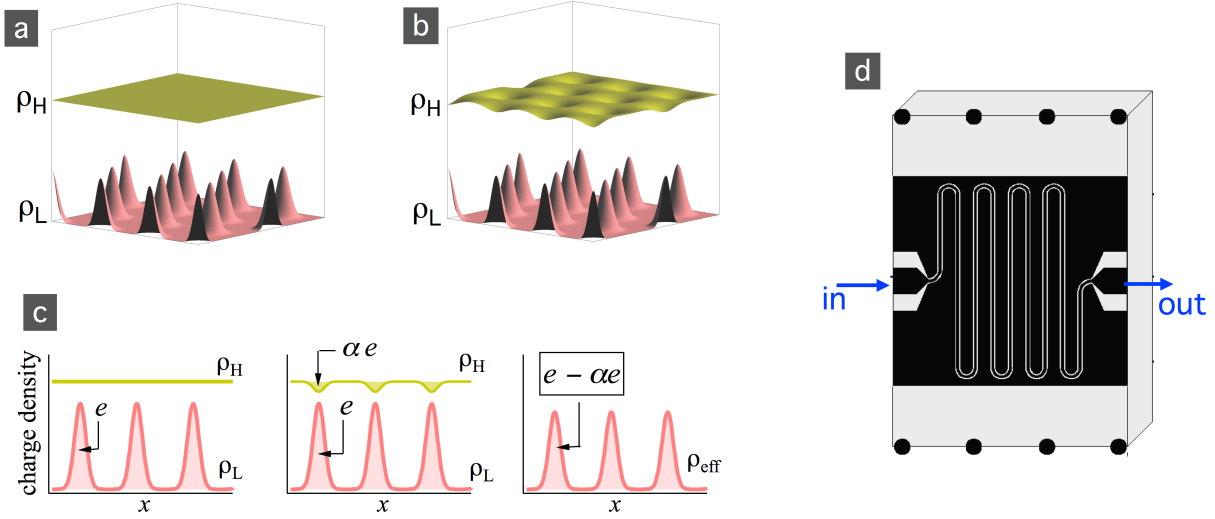


Figure 1: **Wigner solid (WS) close to composite fermion (CF) Fermi sea** The bilayer system has a high-density (majority) top layer that hosts a CF Fermi sea when its Landau filling ν_H is around $1/2$, and exhibits FQHSs at odd-denominator fillings. The low-density (minority) bottom layer has much smaller density compared to the majority layer and forms a WS when the majority layer is in the regime of FQHSs. Panels (a)-(c) show local charge densities of the minority layer and majority layer, $\rho_L(x, y)$ and $\rho_H(x, y)$. (a) The charge densities without screening by the majority layer. ρ_L shows the characteristic triangular Wigner lattice, but ρ_H remains uniform, as in an incompressible liquid state. (b) Same as in (a) but now the majority-layer density screens the WS and develops dimples, regions of locally reduced charge density, which act as opposite-signed “image” charges. (c) Three panels show cuts of figures 1 (a) and (b), through a line of WS electrons of charge e . The left panel is the incompressible-majority-layer situation as in (a). The middle panel shows the static dielectric response of a compressible majority layer to the WS of the minority layer. The dimples, each with charge $-\alpha e$, develop in the majority layer, with $0 \leq \alpha \leq 1$. The right panel illustrates our model of the screened WS: the charge of the image is modeled as summing with the charge at its WS lattice site, creating an effective WS charge per site of $(1 - \alpha)e$. (d) Schematic of the sample used for microwave spectroscopy of WS pinning modes. The dark area is a metal-film coplanar waveguide (CPW) transmission line, through which microwaves are propagated. The CPW has a driven center conductor and grounded side planes, and is capacitively coupled to the electrons in quantum wells. A backgate on the bottom of the sample allows the minority-layer density to be varied.

screening is closest to the dielectric-substrate case rather than the metal-gate case, and can be modeled by image charges less than those at WS sites, as illustrated in Fig. 1.

Experimental Setup

Our samples contain two 30-nm-wide GaAs QWs separated by a 10-nm-thick, undoped barrier layer of $\text{Al}_{0.24}\text{Ga}_{0.76}\text{As}$, giving a center-to-center separation of 40 nm. The QWs are modulation-doped with Si δ -layers asymmetrically: the bottom and top spacer layer thicknesses are 300 nm and 80 nm, respectively. This asymmetry leads to the different 2D electron densities in the QWs. As cooled, the densities of the top, high-density layer and the bottom, low-density layer are $n_{\text{H}} \sim 15$ and $n_{\text{L}} \sim 5.0$, in units of 10^{10} cm^{-2} , which will be used for brevity in the rest of the paper. A bottom gate is used to control n_{L} . As detailed in the Supplement, we obtained n_{H} and n_{L} following the procedure of Deng *et al.* (15, 22), adapted for microwave conductivity measurements using the setup in Fig. 1(d). B -dependent charge transfer between layers for samples like ours is possible, and occurs mainly for $\nu_{\text{H}} > 1$. To account for this, the total density (n_{tot}), which does not change with B , is obtained from low- B Shubnikov-de Haas oscillations, n_{H} comes from high- B majority-layer FQHS positions, and n_{L} in the B range of interest is found by taking the difference between n_{tot} and n_{H} .

Results

The main result of this paper is contained in Fig. 2, which shows pinning modes exhibited by the WS in the minority layer, as B and hence the majority-layer filling, ν_{H} , are varied. The striking feature is that, although the WS resides in the minority layer, the pinning modes are clearly responding to the FQHSs of the majority layer, whose filling ν_{H} is marked at right in the figure. The effect of the majority-layer state on the pinning modes makes it clear that screening of the WS is present. Throughout the measurement range the minority layer filling $\nu_{\text{L}} \leq 0.113$,

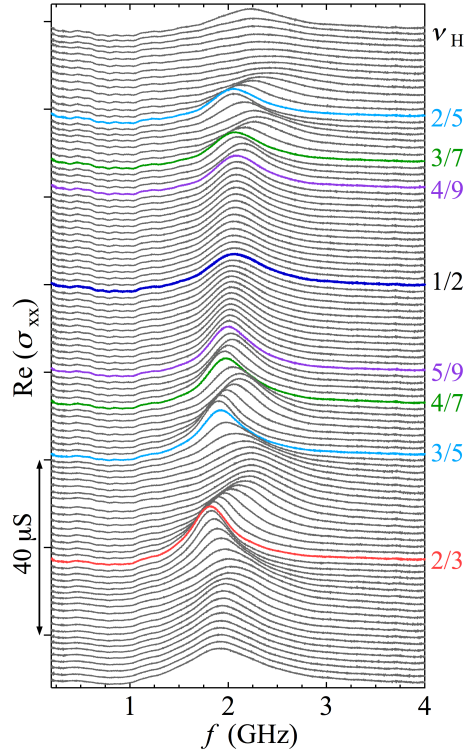


Figure 2: **Pinning mode spectra are strongly affected by majority layer.** $\text{Re}(\sigma_{xx})$ vs frequency, f , spectra at many magnetic fields for majority and minority layer densities $n_H = 15$ and $n_L = 2.20$. Data were recorded in the low-power limit, and at the bath temperature of 50 mK. Traces are vertically offset for clarity and were taken in equal steps of ν_H in the range $0.35 \leq \nu_H \leq 0.75$ ($0.053 \leq \nu_L \leq 0.113$). The majority-layer filling ν_H is labeled on the right axis.

well within the filling-factor range of WS for high-quality, single-layer 2DESs (7, 8, 12–14).

Figure 3(a) illustrates the effect of varying n_L on the pinning mode of the minority layer. $\text{Re}[\sigma_{xx}]$ vs f spectra are shown at different n_L , produced by changing backgate voltage bias. Typical of pinning modes in a single-layer WS at low ν (6, 7, 10), when n_L decreases, the peak frequency f_{pk} increases and the resonance becomes broader and weaker. We will refer to this behavior as the *density effect*. Its explanation in weak-pinning theory (23–25) is that, as the WS softens at lower density, the carrier positions become more closely associated with disorder, and so on average experience a larger restoring force due to a small displacement. The inset of Fig. 3(a) shows the extracted f_{pk} vs n_L . The lines are fits to $f_{pk} \propto n^{-1/2}$; such a dependence

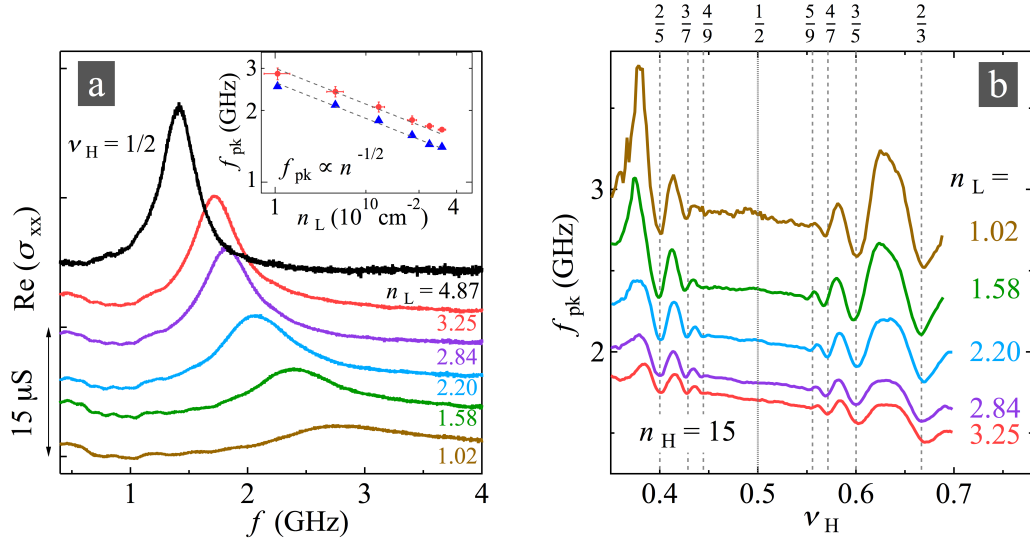


Figure 3: **Pinning mode as minority-layer electron density, n_L , is varied.** (a) $\text{Re}(\sigma_{xx})$ vs f spectra at fixed $\nu_H = 1/2$ ($n_H = 15$) at different n_L . Traces are offset vertically for clarity. The density effect, typical for pinning modes, is evident as decreasing n_L increases f_{pk} , while the resonance amplitude decreases and the resonance broadens. Inset: extracted f_{pk} vs n_L , on a log-log scale, at $\nu_H = 1/2$ (circles) and $2/3$ (triangles). Dashed lines are fits to $f_{pk} \propto n_L^{-1/2}$. (b) f_{pk} vs ν_H at $n_H = 15$ and different n_L ; traces *not* vertically offset. Vertical dashed lines mark rational fractional fillings ν_H of FQHSs. The vertical dotted line marks $\nu_H = 1/2$. The upward overall increase of f_{pk} for each step down in n_L is accompanied by the oscillations of f_{pk} vs ν_H , with minima at majority-layer FQHSs.

has been observed previously (6, 7, 10) for single-layer samples at low densities in the low- ν WS range.

To highlight the clear response of the pinning mode to the majority-layer state, most strikingly the reduction of f_{pk} when a FQHS develops in the majority layer at its odd-denominator fillings $\nu_H = 2/5, 3/7, 4/7, 3/5$ and $2/3$, in Fig. 3(b) we show f_{pk} as a function of ν_H for various n_L . As n_L decreases, the overall f_{pk} curves shift upward over the entire ν_H range. The oscillation amplitudes of f_{pk} seen in Fig. 3(b) at FQHSs of the majority layer become more pronounced when n_L decreases. This is occurring as the spacing of the minority-layer WS electrons exceeds the 40 nm interlayer separation of the double-QW structure. For example, at $n_L = 3.25$ and 1.02 , the triangular WS lattice constant is $a = 60$ and 106 nm, respectively.

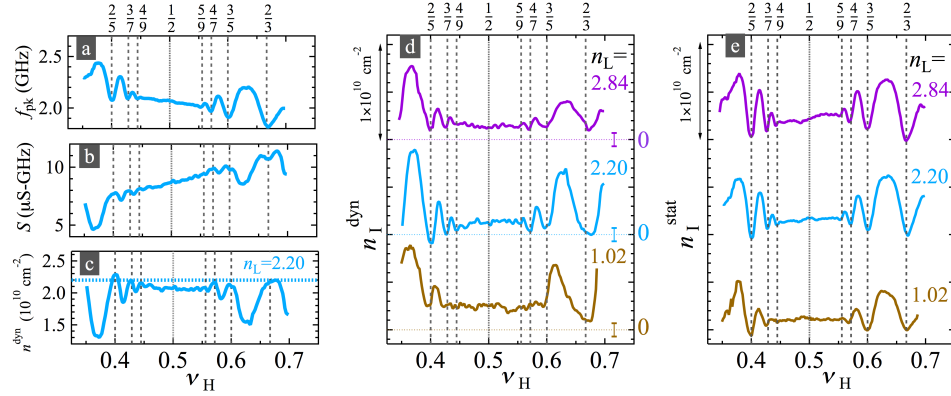


Figure 4: **Effective WS density and image charge densities.** Panels (a)-(c) show plots of several quantities vs ν_H for $n_L = 2.20$, to illustrate the determination of the dynamic effective WS density n^{dyn} : (a) shows f_{pk} , and (b) shows S , the integrated $\text{Re}[\sigma_{xx}]$ vs f , and (c) shows n^{dyn} deduced from the pinning mode sum rule $n^{\text{dyn}} = (2B/\pi e)(S/f_{\text{pk}})$. The overall downward or upward drifts respectively in f_{pk} and S vs ν_H are removed in (c), and a comparatively flat n^{dyn} vs ν_H is observed, in which the FQHSs appear as peaks. (d) shows the density, $n_I^{\text{dyn}} = (n^{\text{dyn}} - n_L)$ of the image charge that moves as the pinning resonance is excited, for three n_L values, plotted vs ν_H . The data are offset for clarity, and the respective zeroes of the traces are shown as lines with error bars. (e) shows the variation of the static image charge density, n_I^{stat} , with ν_H . Traces are offset for clarity.

The FQHS minima in Fig. 3(b) appear on top of a weak decreasing background: for each trace, the f_{pk} oscillations, and also its featureless region between $\nu_H = 0.46$ and 0.54 , are superimposed on a gradual decrease with ν_H . The decrease is similar for each trace, hence insensitive to n_L . In light of this insensitivity, we ascribe the decreasing background to effects intrinsic to the minority layer. For example, such effects could be a change in the WS stiffness (3) or a change in the disorder coupling (23–25) due to a change in the magnetic length (size of the carrier). Single-layer WSs are known to show weak dependence of f_{pk} on B over wide ranges of Landau filling (7).

Discussion

Our interpretation of the data relies on the picture of Fig. 1, in which, above the pinned WS lattice sites in the minority layer, the majority-layer local charge density develops “image” charge minima. The amount of charge in each image depends on the *static* dielectric response of the majority layer, not its conductivity. The ability of the image charge to follow the WS site charge dynamically as the pinning mode is driven, on the other hand, depends on the local conductivity of the majority layer as well. At each WS lattice site, there is then a combination of an image charge with the corresponding charge in the WS. This combined object has a dipole moment, but, because of the finite majority-layer local compressibility, it can also have a nonzero charge. We will characterize our pinning mode data in terms of charge densities. n^{stat} denotes the static charge density of the combined charges, and n^{dyn} denotes the (dynamic) areal charge density that moves as the pinning mode is driven. Like n_L , n^{stat} and n^{dyn} are given in units of 10^{-10} cm^{-2} . A static polarizability, α , as in the caption of Fig. 1, can be defined as $\alpha = n^{\text{stat}}/n_L$.

By means of the pinning mode sum rule (26), $n^{\text{dyn}} = (2B/\pi e)(S/f_{\text{pk}})$, where S is the integrated $\text{Re}[\sigma_{\text{xx}}]$ vs frequency, f , for the resonance. Figures 4(a-c) show, for $n_L = 2.20$, how n^{dyn} is determined: f_{pk} vs ν_H in panel (a) and S from panel (b) produce n^{dyn} in panel (c) by use of the sum rule. S tends to increase as f_{pk} decreases and vice versa. S is increased near the majority-layer FQHS states, reflecting a lack of available cancelling image charge at these low-compressibility states. In panel (c), near the peaks at the most developed FQHSs ($\nu_H = 2/3$ and $2/5$), n^{dyn} approaches n_L , which is shown as a horizontal line. The difference of n_L and n^{dyn} is the image charge density in the majority layer that is moving along with the electrons of the WS, reducing the total current due to the resonance. We call $(n_L - n^{\text{dyn}})$ the dynamic *image* charge density, n_I^{dyn} . It is graphed vs ν_H for $n_L = 1.02, 2.20$ and 2.84 in Fig. 4(d). n_I^{dyn} shows minima at the majority-layer FQHSs, reflecting their small compressibility and small conductivity.

The *static* image charge density n_1^{stat} , obtained as $(n_L - n^{\text{stat}})$, is of particular interest because of its sensitivity to the dielectric response of the majority layer without the influence of the conductivity. It is plotted in Fig. 4(e). While there is no direct method to measure n^{stat} or n_1^{stat} , we can estimate their variations as ν_H sweeps through the FQHSs of the majority layer. We obtain n^{stat} independently from n^{dyn} , from the f_{pk} data of Fig. 3(b) alone. This is possible because in weak-pinning theories (23–25), f_{pk} is solely determined by the stiffness of the WS and the disorder acting on it. Increasing the density of a WS raises its stiffness. As described in the Supplement, the density-effect law, $f_{\text{pk}} \propto n_L^{-1/2}$ is inverted to find n_1^{stat} to within an additive constant. By obtaining n^{stat} from the density-effect law we are treating n^{stat} as if the image charge were on the same layer as the WS; because there is an interlayer separation on the order of the WS lattice constant, this will overestimate the effect of n_1^{stat} , so that the n_1^{stat} we obtain are lower-limit estimates of the true image charge.

A valid low estimate for the absolute n_1^{stat} at $\nu_H = 1/2$, is obtained by neglecting the finite compressibility of the majority layer at $\nu = 2/3$ and taking $n_1^{\text{stat}}(\nu_H = 2/3) = 0$. For the three n_L values of Fig. 4, 1.02, 2.20 and 2.84, we find this low-estimate $n_1^{\text{stat}}(\nu_H = 1/2)$ is about 10% of n_L . The values of $n_1^{\text{dyn}}(\nu_H = 1/2)$ are on the order of their error, also about 10% of n_L . Overall, we find the variations of n_1^{stat} and n_1^{dyn} to be of similar size for most ν_H . This implies that the image charge in the majority layer moves with the WS as the resonance is driven.

In summary we study a WS separated from FQHSs by a distance comparable to its lattice constant. We observe a pinning mode from the minority-layer WS, indicating its existence even in the presence of the nearby, screening majority layer. The pinning mode is strongly affected by the majority-layer FQHSs, exhibiting a reduction in f_{pk} with an increase in S around FQHEs. We find that these phenomena can be modeled by considering image charges in the majority layer, and regarding them as reducing the WS charge. The results indicate that in large part the image charge oscillates as the pinning mode is driven. The image charge is assessed to be about

10% of the WS charge near $\nu_H = 1/2$, but substantially larger elsewhere, particularly at the transitions between FQHSs.

Methods

We performed microwave spectroscopy (6–10) using a coplanar waveguide (CPW) patterned in Cr:Au film on the top surface of the sample. A top view schematic of the measurement is shown in Fig. 1 (d). We calculate the diagonal conductivity as $\sigma_{xx}(f) = (s/lZ_0) \ln(t/t_0)$, where $s = 30 \mu\text{m}$ is the distance between the center conductor and ground plane, $l = 28 \text{ mm}$ is the length of the CPW, $Z_0 = 50 \Omega$ is the characteristic impedance without the 2DES, t is the transmitted signal amplitude and t_0 is the normalizing amplitude. The microwave measurements were carried out in the low-power limit, such that the results are not sensitive to the excitation power at our bath temperature of $T = 50 \text{ mK}$.

Acknowledgements

We thank Ju-Hyun Park and Glover Jones for their expert technical assistance, and J. P. Eisenstein for discussions. The microwave spectroscopy work at the National High Magnetic Field Laboratory (NHMFL) was supported through Department of Energy Basic Energy Sciences (DOE-BES) grant DE-FG02-05-ER46212 at NHMFL/FSU. The NHMFL is supported by National Science Foundation (NSF) Cooperative Agreement Nos. DMR-1157490 and DMR-1644779, by the State of Florida, and by the DOE. The work at Princeton University was funded by the Gordon and Betty Moore Foundation through the EPiQS initiative Grant GBMF4420, and by the DOE BES grant DE-FG02-00-ER45841 and the NSF through grant DMR-1709076 and MRSEC Grant DMR-1420541. Data displayed in this manuscript will be available by email request to engel@magnet.fsu.edu.

Contributions

A.T.H. conceived and designed the experiment, performed the microwave measurements, analyzed the data and co-wrote the manuscript. L.W.E. conceived and designed the experiment, discussed data analysis and co-wrote the manuscript. H.D., Y.L. and M. S. conceived the experiment, discussed data analysis and co-wrote the manuscript. L.N.P., K.W.W. and K.W.B. were responsible for the growth of the samples.

References

1. Y. E. Lozovik, V. Yudson, Crystallisation of a two dimensional electron gas in magnetic field. *JETP Letters* **22**, 11 (1975).
2. K. Yang, F. D. M. Haldane, E. H. Rezayi, Wigner crystals in the lowest Landau level at low-filling factors. *Phys. Rev. B* **64**, 081301 (2001).
3. J.-W. Rhim, J. K. Jain, K. Park, Analytical theory of strongly correlated Wigner crystals in the lowest Landau level. *Phys. Rev. B* **92**, 121103 (2015).
4. E. Y. Andrei, G. Deville, D. C. Glattli, F. I. B. Williams, E. Paris, B. Etienne, Observation of a magnetically induced Wigner solid. *Phys. Rev. Lett.* **60**, 2765–2768 (1988).
5. F. I. B. Williams, P. A. Wright, R. G. Clark, E. Y. Andrei, G. Deville, D. C. Glattli, O. Probst, B. Etienne, C. Dorin, C. T. Foxon, J. J. Harris, Conduction threshold and pinning frequency of magnetically induced Wigner solid. *Phys. Rev. Lett.* **66**, 3285–3288 (1991).
6. C.-C. Li, J. Yoon, L. W. Engel, D. Shahar, D. C. Tsui, M. Shayegan, Microwave resonance and weak pinning in two-dimensional hole systems at high magnetic fields. *Phys. Rev. B* **61**, 10905–10909 (2000).

7. P. D. Ye, L. W. Engel, D. C. Tsui, R. M. Lewis, L. N. Pfeiffer, K. W. West, Correlation lengths of the Wigner-crystal order in a two-dimensional electron system at high magnetic fields. *Phys. Rev. Lett.* **89**, 176802 (2002).
8. Y. P. Chen, R. M. Lewis, L. W. Engel, D. C. Tsui, P. D. Ye, Z. H. Wang, L. N. Pfeiffer, K. W. West, Evidence for two different solid phases of two-dimensional electrons in high magnetic fields. *Phys. Rev. Lett.* **93**, 206805 (2004).
9. G. Sambandamurthy, Z. Wang, R. M. Lewis, Y. P. Chen, L. W. Engel, D. C. Tsui, L. N. Pfeiffer, K. W. West, Pinning mode resonances of new phases of 2d electron systems in high magnetic fields. *Solid State Commun.* **140**, 100 - 106 (2006).
10. Z. Wang, Y. P. Chen, H. Zhu, L. W. Engel, D. C. Tsui, E. Tutuc, M. Shayegan, Unequal layer densities in bilayer Wigner crystal at high magnetic fields. *Phys. Rev. B* **85**, 195408 (2012).
11. I. V. Kukushkin, V. I. Falko, R. J. Haug, K. von Klitzing, K. Eberl, K. Totemayer, Evidence of the triangular lattice of crystallized electrons from time resolved luminescence. *Phys. Rev. Lett.* **72**, 3594-3597 (1994).
12. H. W. Jiang, R. L. Willett, H. L. Stormer, D. C. Tsui, L. N. Pfeiffer, K. W. West, Quantum liquid versus electron solid around $\nu = 1/5$ Landau-level filling. *Phys. Rev. Lett.* **65**, 633–636 (1990).
13. V. J. Goldman, M. Santos, M. Shayegan, J. E. Cunningham, Evidence for two-dimensional quantum Wigner crystal. *Phys. Rev. Lett.* **65**, 2189–2192 (1990).
14. M. Shayegan, in *Perspectives in Quantum Hall Effects*, edited by S. Das Sarma and A. Pinczuk (Wiley-Interscience, New York, 1997), p. 343.

15. H. Deng, Y. Liu, I. Jo, L. N. Pfeiffer, K. W. West, K. W. Baldwin, M. Shayegan, Commensurability oscillations of composite fermions induced by the periodic potential of a Wigner crystal. *Phys. Rev. Lett.* **117**, 096601 (2016).
16. L. Tiemann, T. D. Rhone, N. Shibata, K. Muraki, Nmr profiling of quantum electron solids in high magnetic fields. *Nat. Phys.* **10**, 648-652 (2014).
17. J. Jang, B. M. Hunt, L. N. Pfeiffer, K. W. West, R. C. Ashoori, Sharp tunnelling resonance from the vibrations of an electronic Wigner crystal. *Nature Physics* **13**, 340 EP - (2016).
18. F. M. Peeters, Two-dimensional Wigner crystal of electrons on a helium film: Static and dynamical properties. *Phys. Rev. B* **30**, 159–165 (1984).
19. B. Spivak, S. A. Kivelson, Phases intermediate between a two-dimensional electron liquid and Wigner crystal. *Phys. Rev. B* **70**, 155114 (2004).
20. G. Mistura, T. Günzler, S. Nesper, P. Leiderer, Microwave study of screened two-dimensional electron crystals on helium films. *Phys. Rev. B* **56**, 8360–8366 (1997).
21. J. K. Jain, *Composite Fermions* (Cambridge University Press, Cambridge, 2007).
22. H. Deng, Y. Liu, I. Jo, L. N. Pfeiffer, K. W. West, K. W. Baldwin, M. Shayegan, Interaction-induced interlayer charge transfer in the extreme quantum limit. *Phys. Rev. B* **96**, 081102 (2017).
23. R. Chitra, T. Giamarchi, P. L. Doussal, Pinned Wigner crystals. *Phys. Rev. B* **65**, 035312 (2001).
24. H. A. Fertig, Electromagnetic response of a pinned Wigner crystal. *Phys. Rev. B* **59**, 2120 (1999).

25. M. M. Fogler, D. A. Huse, Dynamical response of a pinned two-dimensional Wigner crystal. *Phys. Rev. B* **62**, 7553–7570 (2000).
26. H. Fukuyama, P. A. Lee, Pinning and conductivity of two-dimensional charge-density waves in magnetic fields. *Phys. Rev. B* **18**, 6245 (1978).

Wigner solid pinning modes tuned by fractional quantum Hall states of a nearby layer: Supplemental Material

A. T. Hatke¹, H. Deng², Yang Liu², L. W. Engel^{1*},
L. N. Pfeiffer², K. W. West², K. W. Baldwin², M. Shayegan²

¹National High Magnetic Field Laboratory, Tallahassee, FL 32310, USA

²Dept. of Electrical Engineering, Princeton University, Princeton, NJ 08544, USA

* to whom correspondence should be addressed, email: engel@magnet.fsu.edu

Obtaining n_H and n_L

We obtained n_H and n_L following the procedure of Deng *et al.* (1,2), adapted for microwave conductivity measurements. For each backgate bias we measured $\text{Re}(\sigma_{xx})$ vs magnetic field, B , at a constant frequency, $f = 500$ MHz, for $0.04 \leq B \leq 0.15$ T. Figure S1 shows a representative trace. The magnetoconductivity exhibits Shubnikov-de Haas oscillations with a fast oscillation corresponding to the majority layer superimposed on a slower oscillation corresponding to the minority layer. The frequencies of the two distinct peaks obtained from a fast Fourier transform, like that shown in the lower inset of Fig. S1, directly yield n_H and n_L , whose sum gives the total density, n_{tot} .

In double quantum wells with unequal densities, increasing B can cause a charge transfer between the layers, particularly until B is large enough that both wells are in the lowest Landau level ($l=3$). We obtain n_H at sufficiently high B for $\nu_H < 1$ through the magnetic-field positions of the well-defined FQHS minima in magnetoconductivity, $\text{Re}[\sigma_{xx}(B)]$, from the majority layer, as shown in the upper inset of Fig. S1. The positions of these minima are consistent with a

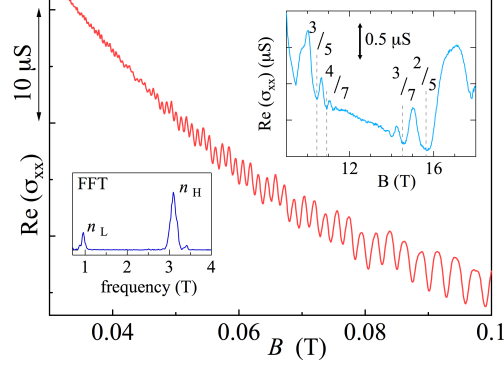


Figure S1: **Data used to determine electron densities of the double quantum well.** Real part of the conductivity, $\text{Re}(\sigma_{xx})$, vs B at fixed microwave frequency, $f = 500$ MHz, which exhibits two oscillation frequencies that correspond to Shubnikov-de Haas oscillations arising from the two wells. The upper inset presents $\text{Re}(\sigma_{xx})$ at high B , exhibiting the majority-layer FQHSs. The lower inset shows the fast Fourier transform (FFT) of the $\text{Re}(\sigma_{xx})$ vs $1/B$ oscillations.

constant high-magnetic-field n_H , indicating to within error of about 1% that there is no charge transfer at high B . Assuming n_{tot} is independent of B , by subtracting the extracted high-field n_H from n_{tot} , we obtain n_L in the magnetic field range of interest.

The possibility of interlayer charge transfer changing the minority-layer density due to the majority-layer FQHSs

The changes in WS density required to produce dips in f_{pk} as we observed are only on the order of a percent or so of the majority layer density, but are of the wrong sign to be explained by static charge transfer driven by the FQHS gap energy, as considered in Refs. (2) and (3). Considering a charge transfer driven by a change of B , the total density change cannot change, so $\delta n_H + \delta n_L = 0$. The change in voltage between the layers due to the transfer is $(e^2/C)\delta n_L = \delta\mu_L - \delta\mu_H$, where C is the geometric interlayer capacitance per unit area, $C = \epsilon\epsilon_0/d$, with d the layer separation. On combining the expressions we find the constant $e^2/C = \delta\mu_L/\delta n_L + \delta\mu_H/\delta n_H$.

For a WS, $\partial\mu_L/\partial n_L$ is expected to be negative, but to increase with n_L . A classical WS (3,4) would have $\partial\mu_L/\partial n_L \propto -n_L^{-1/2}$. At a majority-layer FQHS, $\partial\mu_H/\partial n_H$ exhibits a maximum

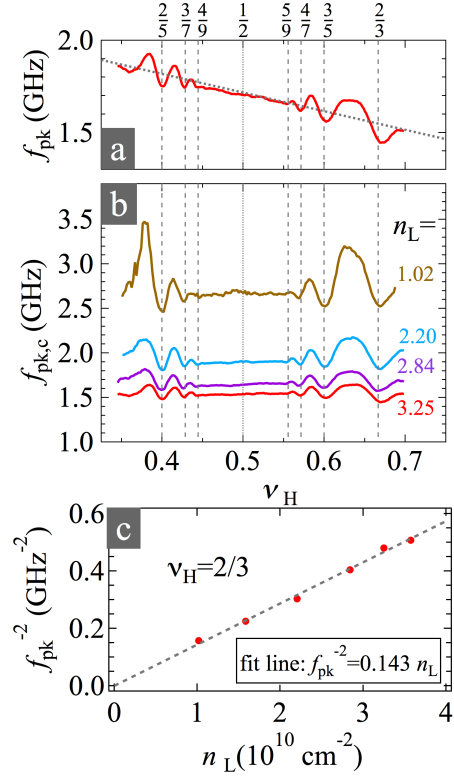


Figure S2: **Fits used to obtain the static image charge density, n_I^{stat} .** (a) f_{pk} vs ν_H , for $n_L = 3.25$, as in Figure 3(b) of the main text. The dotted line is a fit to all data, and its slope is used to subtract off the falling background from f_{pk} vs ν_H traces. (b) The resulting background-subtracted f_{pk} , which we call $f_{\text{pk},c}$ for $n_L = 1.02, 2.20, 2.84$ and 3.25 . (c) The density-effect law, $f_{\text{pk}}^{-2} = \beta n_L$, for the full range of n_L studied. f_{pk} is taken at $\nu_H = 2/3$. β from the fit in (c) is used to compute $n^{\text{stat}}(\nu_H) = \beta^{-1} f_{\text{pk},c}^{-2}(\nu_H)$.

(3), so that a charge transfer would produce a minimum in $\partial\mu_L/\partial n_L$. But in a WS, $\partial\mu_L/\partial n_L$ increases with n_L , so the charge transfer would require a minimum in n_L . This is contrary to our pinning mode data, which imply a maximum in effective WS charge density at a majority-layer FQHS.

Determination of n^{stat} and n_I^{stat} from f_{pk} vs ν_H

We attributed the falling background in Fig. 3(b) of the main text to effects other than screening by the majority layer, so the first task is to remove this background empirically. This is done by

fitting the largest n_L ($n_L = 3.25$) curve in Fig. 3(b) to a line, as shown in Fig. S2(a). $n_L = 3.25$ is chosen because its variations with ν_H are the smallest. A line with the slope of the fit in Fig. S2(a), but set to zero at $\nu_H = 2/3$, is subtracted from the f_{pk} vs ν_H data to remove the falling background, *i.e.* to produce f_{pk} with the background subtracted, $f_{pk,c}$, shown in Fig. S2(b).

We then invert the density effect law to $n^{\text{stat}} = \beta f_{pk,c}^{-2}$ to compute n^{stat} from $f_{pk,c}$, as $\beta^{-1} f_{pk,c}^{-2}(\nu_H)$. β is found from the fit, shown in Fig. S2(c), to $n_L = \beta f_{pk,c}^{-2}$ over the full range of n_L at $\nu_H = 2/3$. Because β is found at $\nu_H = 2/3$, the n^{stat} computed at that filling is fixed to the fit line, which is close to n_L , so that at $\nu_H = 2/3$ n^{stat} is arbitrarily set to near n_L and $n_I^{\text{stat}} = (n^{\text{stat}} - n_L)$ is set to zero.

References

1. H. Deng, Y. Liu, I. Jo, L. N. Pfeiffer, K. W. West, K. W. Baldwin, M. Shayegan, Commensurability oscillations of composite fermions induced by the periodic potential of a Wigner crystal. *Phys. Rev. Lett.* **117**, 096601 (2016).
2. H. Deng, Y. Liu, I. Jo, L. N. Pfeiffer, K. W. West, K. W. Baldwin, M. Shayegan, Interaction-induced interlayer charge transfer in the extreme quantum limit. *Phys. Rev. B* **96**, 081102 (2017).
3. J. P. Eisenstein, L. N. Pfeiffer, K. W. West, Compressibility of the two-dimensional electron gas: Measurements of the zero-field exchange energy and fractional quantum Hall gap. *Phys. Rev. B* **50**, 1760–1778 (1994).
4. G. Fano, F. Ortolani, Interpolation formula for the energy of a two-dimensional electron gas in the lowest Landau level. *Phys. Rev. B* **37**, 8179–8181 (1988).